한국측지학회지, 제 14 권, 제 2 호, pp.127~139(1996년 12월 30일)

Enhanced Recovery of Gravity Fields from Dense Altimeter Data

Kim, Jeong-Hee*

Abstract

This paper presents a procedure to recover sea surface heights (SSH) and free-air (FA) gravity anomalies from dense satellite altimeter SSH data with enhanced accuracies over the full spectrum of the gravity field. A wavenumber correlation filtering (WCF) of co-linear SSH tracks is developed for the coherent signals of subsurface geological masses. Orbital cross-over adjustments with bias parameters are applied to the filtered SSH data, which are then separated into two groups of ascending and descending tracks and gridded with tensioned splines. A directional sensitive filter (DSF) is developed to reduce residual errors in the orbital adjustments that appear as track patterned SSH. Finally, FA gravity anomalies can be obtained by the application of a gradient filter on a high resolution estimate of geoid undulations after subtracting dynamic sea surface topography (DSST) from the SSH. These procedures are applied to the Geosat Geodetic Mission (GM) data of the southern oceans in a test area of ca. 900 km × 1,200 km to resolve geoid undulations and FA gravity anomalies to wavelengths of~10 km and larger. Comparisons with gravity data from ship surveys, predictions by least squares collocation (LSC), and 2 versions of NOAA's predictions using vertical deflections illustrate the performance of this procedure for recovering all elements of the gravity spectrum. Statistics on differences between precise ship data and predicted FA gravity anomalies show a mean of 0.1 mgal, an RMS of 3.5 mgal, maximum differences of 10. 2 mgal and -18.6 mgal, and a correlation coefficient of 0.993 over four straight ship tracks of ca. 1,600 km where gravity changes over 150 mgals.

요 약

본 연구에서는 고밀도 해면고도 자료를 이용하여 모든 스펙트럼에 걸쳐 정밀도가 향상된 해면고도와 중력이상을 계산하였다. 평형 위성궤도상의 해면고도 자료에 주파수 영역에서의 상관계수를 이용한 필터를 적용하여 표층 지각구조에 의한 중력 시그날을 추출하였다. 교점오차를 보정하여 편향 위성궤도 오차를 수정하였으며, 그 결과로 상향및 하향궤도별로 격자상의 중력 시그날을 계산하였다. 또한 방향성 제거 필터를 사용하여 잔재하는 방향성 궤도오차를 수정하였다. 그 결과에 dynamic sea surface topography를 제거하면 지오이드가 되는데 이 지오이드에 gradient 필터를 적용하여 고분해능 중력이상값을 계산하였다. 이 방법들을 약 900 km × 1,200 km지역의 Geosat Geodetic Mission 자료에 적용하여 약 10 km의 분해능을 갖는 지오이드와 중력이상을 계산하였다, 정확한 선상중력 자료와 least squares colloction에 의한 중력이상, 그리고 NOAA의 중력이상값들과 비교, 검토하였다. 약 1,600 km에 걸쳐 150 mgal의 중력변화가 있는 선상중력 측선에서, 본 연구 결과의 중력이상값과 고정밀도 선상중력값을 비교한 결과, 차이의 평균은 0.1 mgal, RMS는 3.5 mgal, 그리고 최대차이는 10.2 mgal과 -18.6 mgal이고, 상관계수는 0.993이었다.

1. Introduction

A significant opportunity for improving our understanding of the gravity field of the oceans has occurred with the release of the Geosat Geodetic Mission (GM) data that provided highly dense coverages over the southern oceans from 60°S to 72°S in late 1990. As well as having a high along-track resolution of 7 km or better, these data have an unprecedented cross-track resolution of about 2~3 km at 60°S, resulting in a significantly enhanced and complete spatial resolution. Clearly, we expect that these data will enable us to predict the ocean's gravity field to a better resolution than was previously available.

* 부산대학교 시간강사

Sandwell (1992) and McAdoo etal. (1992) demonstrated this potential by predicting free-air (FA) gravity anomalies where they claimed resolution of 20 km or better and accuracy at the 5 mgal level. This type of data will be available more and more in the future, not only by further release of the GM data, but also from other altimeter satellites, such as the ERS-1 mission which has been in operation since 1993.

In this paper, for sea surface height (SSH) predictions, a cross-over adjustment will be applied to correct the large orbital errors. Then, we will discuss how to recover accurate medium (ca. 1,000 km) to short wavelength (ca. 10 km) geoid undulations. The resulting geoid undulation will be subsequently used for the prediction of FA gravity anomalies. Free-air gravity anomalies will be predicted using a gradient filter with a small additional correction term. Finally, we will compare prediction results with ground-truthing shipborne gravity data to investigate the quality of these predictions.

2. Data Description and Pre-processing

The GM mission is the primary mission of Geosat that generated unprecedented cross-track ground coverage of 4 km at the equator on 3-day near repeat orbits starting on Apr. 1, 1985 for the duration of 18 months until Sep. 30, 1986 (McConathy and Kilgus, 1987). The resulting 270 million SSHs measured mostly with 0.1 second intervals covering all sea surfaces between 72°S and 72°N (McConathy and Kilgus, ibid.) made it feasible to recover gravity fields of high accuracy and resolution equivalent to those obtained by ship surveying. However, most of these data had been classified since they may provide critical information to Navy operations such as precise mappings of marine gravity field and other key environmental parameters (McConathy and Kilgus, ibid.). In late 1990, the Navy announced partial declassification of the GM data in the southern oceans of 60°S and higher latitudes, which are the data of our interest in this study. More data up to 30°S were further declassified in 1993, and complete release was announced in 1995.

The geophysical dat record (GDR) of the Geosat GM data have the same format as that of the Geosat ERM data also produced by NOAA (Cheney *et al.*, 1987). In each GDR, up to ten 0.1 second SSHs are given, but direct use of each 0.1 second SSH is not desirable due to possible outliers. It is also unnecessary to have high along-track resolution (~0.7 km) by using each 0.1 second SSH, because the cross-track resolution is only 2~3 km at 60°S. In case of ERM GDRs, a straight line fit by least-squares after rejecting 0.1 second SSHs that fail a Tau-test (of 95 % confidence level) was used to form 1 second SSH from up to ten 0.1 second SSHs (Cheney *et al.*, ibid.). ,We also decided to use the same technique, but to form 0.5 second SSHs (~3.4 km) rather than 1 second SSHs (~ 6.8 km) to have the along-track resolution comparable to the cross-track resolution at the region of 60°S and higher latitudes.

The radar altimeter measurements are contaminated with various sources. Corrections for tides (ocean tide: *OCET*, solid earth tide: *SOLT*), atmospheric corrections (dry and wet tropospheric: *DFNOC*, *WFNOC*, ionospheric: *IONO*), significant wave heights (*SWH*), and atmospheric pressure were carried out, resulting corrected SSH (h_c). The total correction term (*TCOR*, in cm) is calculated as follows:

$$\begin{aligned} TCOR &= SOLT+OCET+WFNOC+DFNOC \\ &\quad +IONO-SWH*0.2-9.948* \\ &\quad (PRSR-1013.3)/10 \qquad (2\text{-}1) \end{aligned}$$

where $PRSR = DFNOC/\{-2.277*(1+0.0026*\cos 2\phi)\}$ with ϕ = latitude.

Data on the land or on ice are of no or limited use. Additional editing to remove unreliable data based on GDR parameters were also carried out.

More editings using 3rd order best fitting polynomials were applied, too.

3. Recovery of Accurate Geoid Undulation

The quantity we want to predict first is the geoid undulation which differs from the SSH by the dynamic sea surface topography (DSST) and temporal sea surface changes. A sizable testing area (ca. 900 km by 1,000 km) from 24°E to 42°E longitude and 60°S to 68°S latitude was chosen where good quality ship gravity data are available.

3-1. Wavenumber Correlation Filtering (WCF) on Co-Linear Tracks

An important characteristic of the Geosat GM data is that ground tracks of data points are very dense with separation distance of 2~3 km at 60°S which decreases towards the south pole. Because the water depths up to 72°S are of this order or slightly larger, mass variations as represented by bathymetry and deeper crustal sources produce correlated signals on adjacent tracks which can be extracted by wavenumber correlation analysis. We also expect that uncorrelated parts of h_c due to effects such as noise, time variant signals (seasonal or temporal SSH variations, various corrections, etc.), etc., will be significantly filtered out with this procedure.

The main idea of this method is to decompose space domain data into wave domain coefficients through Fourier transformation, and then construct the correlation spectrum comparing coefficients of a pair (two adjacent tracks) of co-registered (or near co-registered) data at corresponding wavelengths. This comparison is analogous to correlation coefficient (CC) analysis on the regression of the track components in the space domain.

Our strategy is to develop filters based on the correlation spectrum to keep wave numbers if CC is better (greater) than a threshold and discard if

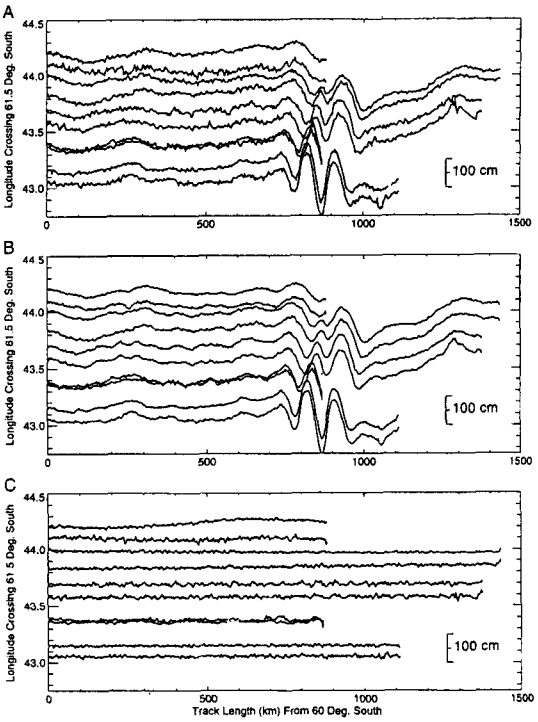

Fig. 1. A) % power retained vs a cut-off CC_k applied in WCF. B) 1st derivative of A) in % power over 0.01 CC_k. An optimal cut-off CC_k may be picked between 0.6 and 0.8.

less. Then, we inversely transform all wave numbers which are highly correlated (i.e., greater than threshold) into space domain. By this approach, negatively and null correlated components including measurement noise, time variant signals, and other incoherent elements are removed so that the coherent signals mostly due to the static subsurface geology are enhanced.

Fig. 1 displays the performance of this filter. Figs. 1-A and 1-B represent residual geoid undulation (SSH subtracted by the OSU91A geoid and OSU91 DSST) over pairs of tracks (5 pairs are displayed) before and after the filtering, respectively. The filtered-out SSHs are shown in Figure1-C. Indeed, the WCF is a procedure to resolve the full spectrum of correlations between co-registered data sets whereas the well-known CC analysis identifies the overall correlation due to the integrated

Table 1. Statistics on the results of cross-over adjustments for 4 sub-prediction blocks

	Block I	Block II	Block III	Block IV
Input Data Point	86,327	88,906	87,492	85,545
& Tracks	734	720	755	727
Mean & RMS(cm) w.r.t OSU91A	-9.3±55.9	-5.8±56.3	-4.1±61.7	-0.1±62.8
Ouliers & peaks	2,245	2,572	2,475	2,655
Tracks used in Adjustment	681	684	703	675
(total/Desc/Asc)	371/315	383/301	380/323	368/307
Cross-over Points	32,896	35,255	33,305	33,558
Mean & RMS (cm) of Cross-over	-24.5±72.0	-17.8±73.7	-30.0±76.0	-26.9±78.3
before adjustment after adjustment	1.1±7.8	0.5±7.8	1.9±8.0	1.1±8.0

effect of the spectral components.

3-2. Cross-over Adjustment

Through co-linear analysis, various measuring errors, correction errors, and orbital errors of medium to short wavelengths that caused inconsistencies among neighboring tracks appear to be mostly removed. However, the largest error of all is the long wavelength orbital errors, which may require complicated and laborious computations to correct. To reduce orbital errors, cross-over adjustment techniques have been in wide use (e.g., Rapp,1985) for Geos-3 and Seasat altimeters. This approach involves linear systems of one rank defect for datum, an imperfect stochastic model, and it neglects the time history of orbits (for example, Rummel (1992) and Knudsen (1987)). However, they can reduce significant parts of radial orbit errors when applied to regional areas of scales of 1,000 km by 1,000 km.

The test area is divided into 4 overlapping adjustment blocks of 12°W-E by 6°S-N with 2° borders. Input data for the adjustment are the filtered ARG. This filtered ARG is the SSH after removing the geoid of OSU91A 360° field and SST of OSU91 SST model, and then filtered through the co-linear analysis. Actual adjustments are carried out using the program ALTCOR developed by Knudsen and Rapp at the Ohio State University.

Table 1 shows the results of adjustments for the test area. The RMS of cross-over differences is about 8 cm or less for an adjustment block typically with ~ 86,000 data points and ~ 33,000 cross-over points. This RMS is substantially improved by ~ 7 cm over the results obtained with no co-linear filtering. Considering the effects of the extensive ice coverage and large SWH of the southern oceans, this RMS is satisfactory. For reference, the RMS of the Seasat altimeter data, which has similar data quality to Geosat's, is ~ 10 cm level for a similar size of adjustment blocks (Basic & Rapp, ibid., p. 47) dispite adjusting with much less data points observed over the better conditioned Northern Pacific Ocean.

3-3. Directional Sensitive Filter (DSF)

The WCF technique was designed to remove significant part of noise and time signals which are not consistent (and hence not geologic) between adjacent co-linear tracks. This WCF approach can be implemented on a 2-dimensional (2-D) basis to extract coherent signals between predictions produced from data sets of descending and ascending groups. This procedure is very effective in further decreasing the noise-to-signal ratio, since each data set group, when predicted using descending only and ascending only, will reflect different characters of non-static signals in h_c. In predictions, these non-

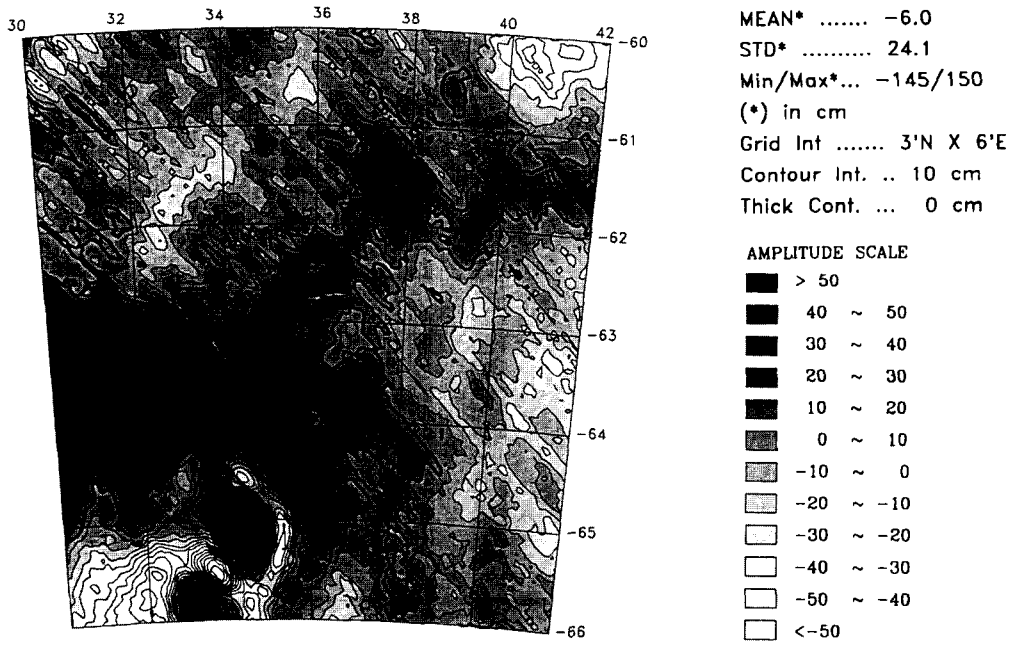

Fig. 2. Residual geoid undulation predicted from ascending groups of GM data gridded using the tensioned cubic spline method after applying co-linear track filters and cross-over adjustment. The OSU91A Earth gravity model and the OSU91 DSST model of harmonic coefficients degree and order 360 and 10, respectively, are removed.

static signals appear as washboard effects perpendicular to the track orientations (see Fig. 2).

To minimize the track-patterned effect, we designed a directional sensitive filter whereby we replaced those wavenumbers contaminated by the track-like non-static signals from one set of predictions with wavenumbers from another set of predictions that were not contaminated by the errors of the same directional type. In this filter, the power spectra contents of the two data sets must be very close in terms of total power and *N/S*. In conclusion, we decided to exchange the entire 2 quadrants of wavenumbers of contaminated patterns from one data set with 2 uncontaminated quadrants of wavenumbers from the other data set, and then constructed one complete wavenumber array that essentially contains no wavenumber components with strong track pattern distortions.

Fig. 2 shows predicted ARG gridded by the tensioned cubic spline method at 3' by 6' in meridian and parallel direction, respectively, using data on ascending tracks only after the WCF on co-linear tracks and cross-over adjustments were applied. The resulting space domain ARG afer the DSF was applied is shown in Fig. 3. Visual inspection of Figs. 2 and 3 reveals that most track patterned short wavelength inconsistencies across tracks are now removed without introducing any additional sstematic errors. The total geoid undulation field can be calculated merely by adding the OSU91A reference undulation.

4. Free-Air Gravity Anomaly Prediction

Thus far, we have completed the predictions of the ARGs over a 8° (meridian) by 18° (parallel) block (~700 km by ~700 km) using four sub-blocks gridded at 3' by 6' (also in meridian and parallel direction, respectively) intervals (~5.5 km by ~5.5 km). The next step is to derive residual

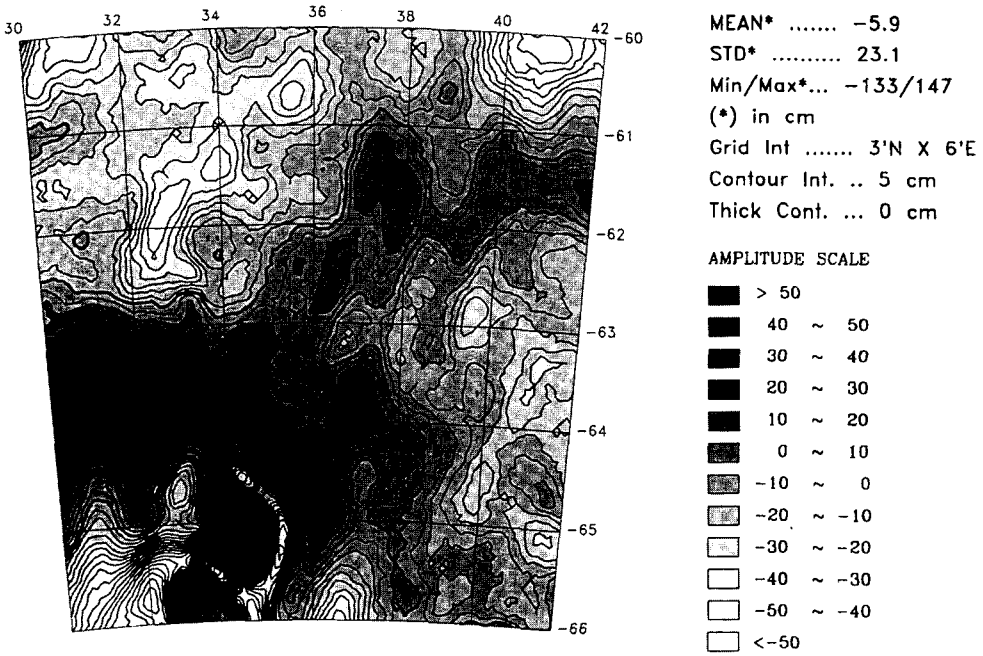

Fig. 3. Residual geoid undulation after the directional sensitive filtering is applied on a prediction set of ascending groups of GM data (Fig. 1) and that of descending groups of GM data.

FA gravity anomalies from the ARGs through the method based on the fundamental equation of geodesy. The total FA gravity anomalies can be found by adding the reference anomalies of the OSU91A to these predictions.

4-1. Direct Conversion of Geoid Undulation to FA Gravity Anomaly

The fundamental equation of physical geodesy (Heiskanen & Moritz, ibid., p.112) when combined with Brun's formula (Heiskanen and Moritz, ibid.) after reasonable approximations gives the direct relation between geoid undulations and gravity anomalies as follows:

$$\Delta g = -\frac{\partial T}{\partial r} - \frac{2}{R}T = -\frac{\partial}{\partial r}(N\gamma)\frac{2}{R}(N\gamma) \qquad (4\text{-}2)$$

where T is the disturbing potential, N is the geoid undulation, γ is the normal gravity and R is the radius of the earth. The first term on the right hand side of (2) is called the gravity disturbance (δg) that can be calculated by the FFT technique using satellite altimeter SSH for N. This SSH differs from N by dynamic sea surface topography (DSST) and this difference will result in a minimal errors in this term as DSST generally has a characteristics of long wavelengths to 1,000 km or more. The second term is also calculated from the observed SSH and errors in this term due to DSST can be reduced using a reasonable DSST model, such as the OSU91 DSST model to degree and order 10 that is applied in this study. Residual errors in DSST and other factors may cause additional small errors, e.g., 30 cm error will be converted to 0.1 mgal.

Consider N as given on uniformly spaced grids (discrete data). Since T is a harmonic function, it satisfies the Laplace's equation,

$$\frac{\partial^2 T}{\partial x^2} + \frac{\partial^2 T}{\partial y^2} + \frac{\partial^2 T}{\partial z^2} = 0 \qquad (4\text{-}3)$$

For T on the x-y plane, the 2-D inverse Fourier transform gives

$$T(x,y)=\frac{1}{MN}\sum_{k=0}^{M-1}\sum_{l=0}^{N-1}\bar{T}_{kl}e^{j(k\frac{2\pi}{M}x+l\frac{2\pi}{N}y)} \quad (4\text{-}4)$$

where $\bar{T}_{kl}$ is the 2-D Fourier transformation of T_{xy}. Taking second derivative of T_{xy} in (4) with respect to x gives

$$\frac{\partial^2 T}{\partial x^2}=\sum_{k=0}^{M-1}\sum_{k=l}^{N-1}\{-(k\frac{2\pi}{M})^2\}\bar{T}_{kl}e^{j(k\frac{2\pi}{M}x+l\frac{2\pi}{N}y)} \quad (4\text{-}5)$$

and similarly with respect to y, we have

$$\frac{\partial^2 T}{\partial y^2}=\sum_{k=0}^{M-1}\sum_{k=l}^{N-1}\{-(l\frac{2\pi}{N})^2\}\bar{T}_{kl}e^{j(k\frac{2\pi}{M}x+l\frac{2\pi}{N}y)} \quad (4\text{-}6)$$

Plugging (6) and (5) into (3) and rearranging gives

$$\frac{\partial^2 T}{\partial z^2}=\frac{1}{MN}\sum_{k=0}^{M-1}\sum_{k=l}^{N-1}\{(k\frac{2\pi}{M})^2+(l\frac{2\pi}{M})^2\}\bar{T}_{kl}e^{j(k\frac{2\pi}{M}x+l\frac{2\pi}{N}y)}$$
$$=\frac{1}{MN}\sum_{k=0}^{M-1}\sum_{k=l}^{N-1}\kappa\bar{T}_{kl}e^{j(k\frac{2\pi}{M}x+l\frac{2\pi}{N}y)} \quad (4\text{-}7)$$

where $\kappa=(k\frac{2\pi}{M})^2+(l\frac{2\pi}{M})^2$. Comparing (7) with (4), we find that (is the coefficient of the Fourier wavenumber ($\bar{T}_{kl}$) for the 2nd derivatives of T_{xy}. Thus, we can rewrite (7) as

$$\frac{\partial^2\bar{T}_{kl}}{\partial z^2}=\kappa\bar{T}_{kl}. \quad (4\text{-}8)$$

The condition, , constrains the solution of (8) to

$$\bar{T}_{kl}=Ce^{-\sqrt{\kappa}z} \quad (4\text{-}9)$$

where C is an arbitrary constant. Then, the first vertical derivative of (9) gives the Fourier wavenumber of δg as,

$$\delta\bar{g}_{kl}=-\frac{\partial\bar{T}_{kl}}{\partial z}=-(-\sqrt{\kappa}Ce^{-\sqrt{k}z})=\sqrt{\kappa}\bar{T}_{kl} \quad (4\text{-}10)$$

Finally, δg is calculated by the inverse Fourier transformation of (10) as

$$\delta g=\frac{1}{MN}\sum_{k=0}^{M-1}\sum_{l=0}^{N-1}\sqrt{\kappa}\bar{T}_{kl}e^{j(k\frac{2\pi}{M}x+l\frac{2\pi}{N}y)} \quad (4\text{-}11)$$

In reality, data ($T=\gamma N$) are given on the ellipsoid with geographical coordinates system (ϕ, λ) for the limited area so that a few approximations are involved in actual computations as follows:

1) planar approximation : $\partial/\partial z=\partial/\partial r$

2) map projection approximation : $(\varphi, \lambda)\Leftrightarrow(x,y)$

3) neglecting the remote zone effect due to use of limited areal data.

However, since FFT technique of a gradient filter for gravity prediction is a high-pass filter operation applied for a small calculation area of 1,000 km by 1,000 km or less, effects of all these 3 approximations are expected to be minimal. Note that in the extreme case of pole regions, the effect of 3) can be very significant, so that the proper projection must be applied (e.g., azimuthal projection with the center of projection being in the middle of the calculation area).

In fact, the most significant error source of applying a gradient filter is the edge effect. This edge effect is caused by discontinuities of opposing data edges of the prediction area when a Fourier transformation is applied. It may result in an unreasonable prediction with a large magnitude and high frequency due to the characteristic high-pass filter behavior of our method. The predictions on the edges of the calculation area will be less reliable than those toward the middle of the area. This effect can be reduced by introducing a reference undulation field that fits the observed undulation. With a reference undulation field (N_{ref}), (2) can be re-written as,

$$\Delta g=-\frac{\partial}{\partial r}(N_{ref}+N_{res})\gamma-\frac{2}{R}(N_{ref}+N_{res})\gamma$$
$$=-\frac{\partial(N_{ref}\gamma)}{\partial r}-\frac{2}{R}N_{ref}\gamma=\{-\frac{\partial(N_{res}\gamma)}{\partial r}-\frac{2}{R}N_{res}\gamma\}$$
$$=\Delta g_{ref}+\Delta g_{res} \quad (4\text{-}12)$$

where subscripts ref and res indicate reference field and residual field, respectively. From (12), the role of the reference gravity model is to approximate the actual field so that the residual term would have smaller edge effects and, consequently, improve the prediction. Further numerical en-

gineering efforts, such as folding-out and proper window carpentry of the data also will help reduce edge effect.

4-2. Test Prediction

A 2-D gradient filtering program was developed for free-air gravity anomaliy predictions. The input data are predicted ARG and the output is residual free-qir gravity anomalies (Δgres in (12)) as the correction term (the second term in (2)) was also added in the program. The total FA gravity anomalies can be found by adding the reference FA gravity anomalies of the OSU91A to these predictions.

The predicted residual FA gravity anomalies have unreasonable high frequency components, and we applied a low-pass filter on the FA gravity anomaly predictions to remove them. It was only necessary to suppress the shortest of these wavelengths to be sufficient enough to remove those components. The order used here was a transformation of the ARG to FA gravity anomalies, followed by a low pass filtering of the anomalies. It should be noted that there is no difference in the resulting predictions if the ARG is low pass filtered first and then used to determine the FA gravity anomalies, indicating a stable relationship between the ARG data and the FA gravity anomaly predictions. The resulting FA anomalies have a resolution of ~ 10 km.

A principal cause of edge effects is the discontinuity of the input values that occurs along the prediction block boundaries. An assumption in applying the Fourier transformation is that the field must repeat itself at the boundaries, which is not the case in practice for the blocks used in predicting the Earth gravity field. This discontinuity at the opposite edges of the blocks will result in bad predictions because the prediction process of a gradient filter is essentially a high-pass filtering operation. To reduce these effects, we should apply a reference field that fits the actual gravity field (undulation) well so that the edge mismatches become smaller. In this study, the OSU91A geoid undulation and the OSU91 SST field were applied, resulting in the ARG field. In fact, another Earth gravity model was also used as a reference field (GEM-T2 to degree 50 incomplete) for comparison. In general, the resulting predictions were very consistent between the two reference fields near the middle of prediction areas where edge effects are minimal. Lower degree models of the OSU91A were tried too, and the results were similar. The only difference among the predictions using different reference gravity models is the magnitude of edge effects. In general, the better a reference gravity model fits the altimeter measured SSHs, the less are the edge effects that occur.

A good fitting reference field reduces edge mismatches tremendously (from a few meters to a decimeter level), but they are still large enough to cause unreliable predictions at and near edges. Another step to reduce them further is to smooth ARGs near edges by applying an appropriate window that tapers and forcing the ARG edges to the zero. However, applying a window will yield artificially smoothed ARGs that also may result in distorted predictions. Various windows with different lag parameters were tried, but found to yield unreliable predictions which looked washed out toward edges and/or were not consistent with predictions of neighboring blocks. The procedure we adopted to solve this problem involves folding out the ARGs along the edges, making fields that are 4 times larger, and symmetric along the edges. By this process, the ARGs are continuous at the original edges, and the application of windows on the enlarged edges will not cause any serious problem for the predictions at the original prediction area in the middle. A remaining problem was due to abrupt changes of the ARGs at the original edges, in the case where the ARGs at the edges have considerable slopes. In this instance, predictions at these edges will be unstable with relatively large magnitudes, but they restricted to within a few

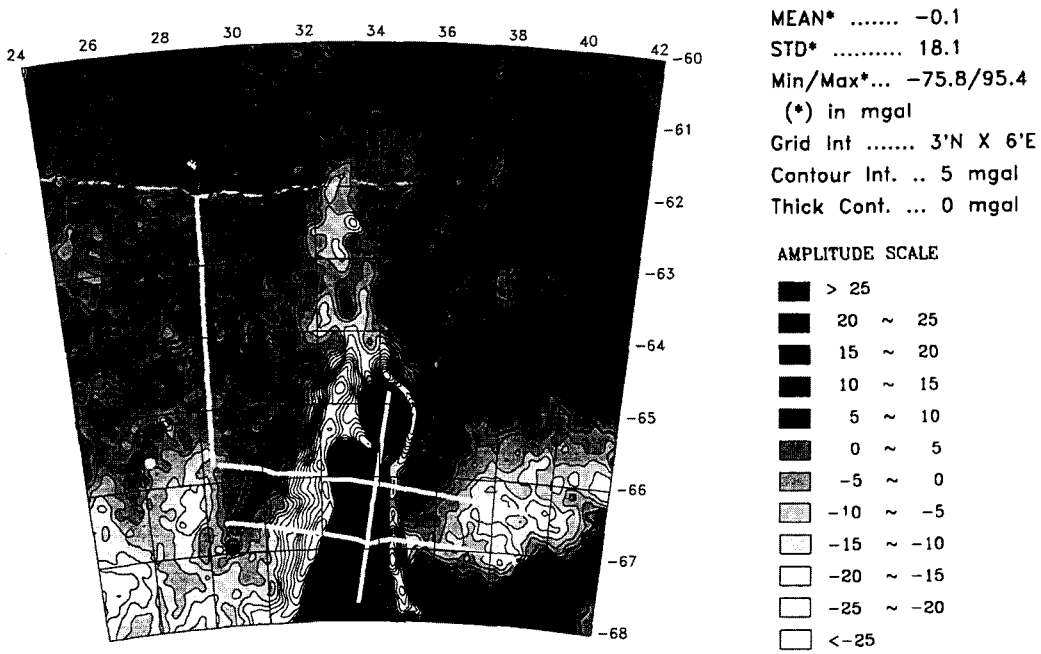

Fig. 4. Locations of 4 near straight ship tracks for comparsions. Predicted total anomalies of the WCF method are shown.

rows or columns the edges.

These erratic predictions at the original edges can be identified and also their magnitude can be assessed by comparing predicted values of neighboring blocks. We made FA gravity anomaly predictions of two neighboring blocks with overlapping halves. The predictions near edges are very different, especially right on the edges having erratic values of very large magnitudes. But, the predictions at the 10th column (of 128 prediction columns) inward from the edges are very consistent with a RMS difference of only 0.5 mgal. We must note that these differences also include the effects of using different groups of ARGs in each block and of neglecting the remote zones. Again, these effects on FA gravity anomaly predictions by the high-pass filterings are confirmed to be minimal.

Fig. 4 shows a map of predicted total FA gravity anomalies that include reference anomalies. It also shows the statistics for the test area. Four thick white lines are ship tracks where good shipborne gravity is available for comparisons in the next chapter. The standard deviation (STD, magnitude) of recovered FA gravity anomalies from ARG is around 14 mgals, and this magnitude is about 140 % of that of the reference field. This value is much larger than the reported percentage of power in this and shorter wavelengths (estimated to 40%). It is due to the strong gravity field generated by a seamount-like structure around 34°E longitude and 65°S latitude.

The method does not yield analytical error estimations, but errors seem to be roughly 3 to 5 mgals when compared to good quality shipborne data (see the next chapter for details). In the next chapter, these test predictions are compared with shipborne and other available data to check the quality of this method.

5. Comparison of Altimetry Derived Free-Air Gravity Anomaly Prediction

Insight on the errors in estimating FA gravity anomalies from altimetry SSH may be obtained by

comparing the results of the various prediction methods against good quality ship-borne measurements. In general, ship-borne gravity surveys readily show drift error of c.a. 10 mgal level at the cross-over shipborne measurement locations (Wessel, Watts, 1992), and hence are not useful for comparing with altimeter derived gravity data. Fortunately, a shipborne data set with the prerequisite accuracy was collected for this study, by the 1990 cruise of the BGR (Bundesanstalt fur Geowissenschaften und Rohstoffe) ship "Polar Stern". The BGR kindly provided with this shipborne gravity data (Rapp, personal communication) that had relatively small drift error (ca. 2~3 mgal) over the entire cruise of some 8,000 km. We confirmed the magnitude of the overall error including the drift error by checking the shipborne FA gravity anomaly measurements at numerous cross-over points. They were mostly within 1 mgal except on 2 occasions when the differences reached the 2 mgal level in areas where strong anomaly maxima occurred. Furthermore, the initial comparison showed no sign of tilts or biases that were correlated with ship's headings. In summary, we believe the accuracy of the BGR data to be 2 mgal or better, which makes these data very suitable for the purpose of accurate comparison.

Four essentially straight ship tracks were chosen for comparisons as shown in the Fig. 4. Two of the ship tracks run approximately from west to east (WE1 and WE2, near 66°S and 67°S, respectively), and the other two tracks run approximately from north to south (NS1 and NS2, near 28.5°E and 34°E, respectively). The three tracks of WE1, WE2, and NS2 pass over the areas of dramatic gravity variations, whereas track NS1 passes over a nearly flat gravity field. Because cruise distances between measurements are only around 0.2 km, we took BGR data at every 10th point for the comparison. The number of comparison points range from 188 to 270 points and track lengths ranging from 330 km to 490 km, which are sufficiently

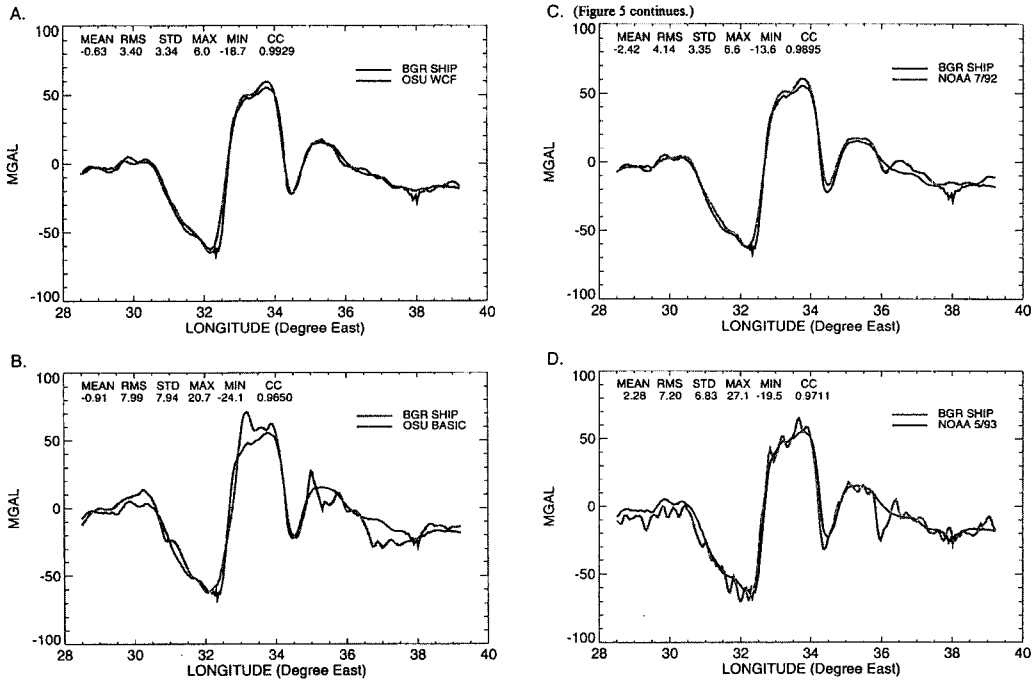

Fig. 5. FA geavity anomalies on a ship track WE1. BGr data and A) OSU WCF, B) OSU BASIC, C) NOAA 7/92, and D) DOAA 5/93 are shown. Statistics are for BGR-predictions in megal except CC

long to check any significant biases and/or trends.

Fig. 5 compares the ship data (BGR) with results of this study (OSU WCF) and 3 other data sets along profiles WE2. The other 3 data sets are results from least squares collocation (OSU BASIC) generated here at OSU (Basic and Rapp, 1992), and results obtained by NOAA and distributed publicly in July 1992 (NOAA 7/92) and May 1993 (NOAA 5/93). Note that the LSC results are based on ERM and Seasat data only and do not include GM data whereas NOAA's results were by using Geosat GM and ERM data. Elements of these prediction methods are shown in Table 2. This figure gives four comparisons including : A) BGR and OSU WCF, B) BGR and OSU BASIC, C) BGR and NOAA 7/92, and D) BGR and NOAA 5/93. Table 3 shows important statistics for these data that characterize their differences with respect to the BGR ship data. In the table, the slope is that of the best fitting straight line to differences between predictions and shipborne data and it may depict a tilt-like long wavelength error characteristics.

Study of Table 3 and Fig. 5 shows that the OSU WCF data in general compare significantly more favorably with the BGR shipborne data than the other three data sets. The NOAA 7/92 data represent the next most favorable comparison along the ship tracks. On WE1 and WE2, important statistics including the mean, RMS, and correlation coefficient show that the OSU WCF results represent marked improvements over other results when compared to the BGR data. On WE1, the RMS of the OSU WCF results shows 18%, 53%, and 58% improvement over NOAA 7/92, NOAA 5/93, and OSU BASIC, respectively, and the CC is improved by 0.4%, 2.2%, and 2.8%. On WE2, the RMS is improved by 83%, 36%, and 52%, and the CC is improved by 0.7%, 12.6%, and 1.5%. For track NS2,

Table 2. Statistics of comparisons on 4 selected ship tracks (WE1, WE2, NSI, & NS5) between BGR (shipborne) and, 1) WCF, 2) BASIC, 3) NOAA 7/92, & 4) NOAA 5/93.

	Mean(mgal)	RMS(mgal)	STD(mgal)	Min/Max(mgal)	Slope(mgal/100 km)	CC
WE1						
BGR-WCF	-0.63	3.40	3.34	-18.7/ 6.0	-0.29	0.9929
BGR-BASIC	-0.91	7.99	7.94	-24.1/20.7	1.43	0.9650
BGR-NOAA 7/92	-2.42	4.14	3.35	-13.6/ 6.6	-1.04	0.9895
BGR-NOAA 5/93	2.28	7.20	6.83	-19.5/27.1	-1.44	0.9711
WE2						
BGR-WCF	-1.09	3.04	2.83	-13.0/ 8.5	0.08	0.9959
BGR-BASIC	-1.62	6.37	6.16	-13.9/24.0	2.32	0.9807
BGR-NOAA 7/92	-3.33	4.88	3.57	-18.8/ 4.7	-1.38	0.9889
BGR-NOAA 5/93	4.02	7.46	6.28	-10.9/20.2	-2.91	0.9778
NS1						
BGR-WCF	0.31	2.01	1.99	-4.8/ 4.9	-0.38	0.9359
BGR-BASIC	3.30	4.73	3.38	-4.8/12.4	0.41	0.8696
BGR-NOAA 7/92	1.41	2.14	1.62	-1.9/ 6.5	-0.14	0.9416
BGR-NOAA 5/93	3.30	4.73	3.38	-4.8/12.4	0.91	0.8696
NS2						
BGR-WCF	-3.29	5.51	4.42	-15.2/10.2	-0.12	0.9953
BGR-BASIC	-2.10	10.91	10.70	-27.3/27.0	4.79	0.9795
BGR-NOAA 7/92	-4.53	6.01	3.96	-11.6/6.6	-2.38	0.9948
BGR-NOAA 5/93	-0.80	8.68	8.65	-20.2/23.0	4.66	0.9826

Table 3. Elements of Prediction Methods

	OSU WCF	OSU BASIC	NOAA 7/92	NOAA 5/93
data used	Geosat GM	Seasat Geosat ERM	Geosat GM Geosat ERM	
data processing	WCF co-linear track filtering	bathymetric information added	Gaussian smoothing on η, ξ	optimal FIR differentiators on along track SSH
method	conversion of geoid undulation $\Delta g = -\gamma\frac{\partial N}{\partial M} - \frac{2\gamma N}{R}$	collocation	conversion of vertical deflection gravity disturbance is calculated $\frac{\partial \Delta g}{\partial z} = -\gamma\left(\frac{\partial \eta}{\partial x} + \frac{\partial \xi}{\partial y}\right)$	
reference field used	OSU91A 360 OSU91 10 DSST	OSU91A 360 OSU91 10 DSST	GEM-T2 50 no DSST	
comments	planar approx., map approx. better integrity in all wavelength	limited data predicated on smaller block border problems among prediction cells	planar approx., map approx. partial gravity disturbance less fidelity in mid to long wavelengths contamination in short wavelength	

OSU WCF represents 8%, 37%, and 49% improvement in the RMS, and also represents 0.1%, 1. 3%, and 1.6% improvement in the CC, although its predictions at anomaly maxima are overestimated by 13% or 10.2 mgals at near 65(S latitude. Note that on these 3 tracks, FA gravity anomalies vary over 100 mgals along only about 300 ~ 500 km which represents a very rough marine gravity field. On NS 1, where the gravity field is very smooth (varying only about 20 mgals), the results of OSU WCF and NOAA 7/92 are both equally more comparable to the BGR data than those of two others. Both NOAA 5/93 and OSU BASIC result are marginally less comparable to the ship data. NOAA 5/93 is much less comparable than the previous result of NOAA 7/92. OSU BASIC was calculated with incorporation of ETOPO5U bathymetry effects, but without dense GM altimeter data, and yielded the least comparable results.

6. Conclusions and Recommendation

The goal of this study was to develop an improved method for predicting geoid undulations and FA gravity anomalies from satellite altimeter data. This study has advanced this objective significantly using geological constraints of extracting static (time invariant) geological signals in SSHs that are embodied in the application of WCF for co-linear track filtering and track-pattern detrending filters, as well as geodetic constraints for orbital adjustments and effective co-phasing of the data tracks. The comparisons with high quality shipborne data show our predictions to have an RMS difference of 3.5 mgals with minimal systematic errors. This accuracy is close to the theoretical accuracy limit of 3 mgals reported for the Geosat data from a coherency analysis of hundreds of exact repeat orbits by Sailor and Discoll (1993). The accuracy may be well improved at lower latitudes, where the effects of ice and SWHs are less and, consequently, the quality of GM data are better. In general, the procedure of this study appears to produce the gravity fields of significantly enhanced and consistent FA gravity anomalies with substantially improved resolution and ac-

curacy, as well as geologically consistent geoid undulation of wavelengths from 10 to 1,000 km. Meanwhile, the resolution of predicted FA gravity anomalies is ~ 10 km. As more altimetry missions are completed and the coverage of world oceans improves, the continued implementation of the procedures developed in this research will yield improved understanding of the marine gravity anomaly field.

Although our efforts were very satisfactory, there are a few more steps to take that may improve efficiencies and qualities of the predictions. The far most important step is believed to make the gradient filter work for geographical coordinates of ϕ and λ without planar approximations. Because of this approximations, the size of the gravity anomaly (more precisely, gravity disturbance) prediction area is limited, and small systematic long wavelength errors are included in the predictions. We have already started to look at solving this problem. Our suggestion is first to apply the FFT along one direction (either meridian or parallel) line by line, and then to sum up those results. This is similar to a method (ref.) whereby gravity anomalies were used to recover geoid undulations. However, the gradient filtering (the inverse of the reference's method) from geoid undulations to gravity anomalies has not yet been attempted.

Acknowledgment

The financial support for this study was provided by Korean Science and Engineering Foundation, Project No. 95-0703-01-01-3.

References

1. Basic, T. and R.H. Rapp, Oceanwide prediction of gravity anomalies and sea surface heights using Geos-3, Seasat, and Geosat altimeter data and ETOPO5U bathymetric data, Report No. 416, Department of Geodetic Science and Surveying, The Ohio State University, Columbus, Ohio, 1992.
2. Cheney, R.E., B.C. Douglas, R.W. Agreen, L. Miller, D.L. Porter and N.S. Doyle, Geosat Altimeter Geophysical Data Records-User Handbook, NOAA Technical Memorendum NOS NGS-46, Rockville, Maryland, 1987.
3. Heiskanen, W.A. and H. Moritz, Physical Geodesy, Freeman anf Company, San Francisco, CA, 1967.
4. Knudsen, P., Adjustment of satellite altimeter data from from cross-over differences using covariance relations for the time varying components represented by Gaussian functions, Proc. IAG Symposia, TOME II, p. 617-628,1987.
5. Marsh, J.G., F.J. Lerch, B.H. Putney, T.L. Felsentreger, B.V. Sanchez, S.M. Klosko, G.B. Patel, J.W. Robbins, R.G. Williamson, T.L. Engelis, W.F. Eddy, N.L. Chandler, D.S. Chinn, S. Kapoor, K.E. Rachlin, L.E. Braatz, and E.C. Pavlis, The GET-T2 Gravitational Model, J. Geophys. Res., Vol. 95, No. B13, p.22043-22071, 1990.
6. McAdoo, D.C. and K.M. Marks, Gravity field of the southern ocean from Geosat data, J. Geophys. Res., vol. 96, No. B3, 1992, pp. 3247-3260.
7. McConathy, D.R. and C.C. Kilgus, The Navy Geosat Mission : An overview, Johns Hopkins APL technical digest, vol. 8, No. 2, pp.170-175, Laurel, Maryland, 1987.
8. Rapp, R.H., Detailed gravity anomalies and sea surface height derived from Geos-3/Seasat altimeter data, Report No. 416, Department of Geodetic Science and Surveying, The Ohio State University, Columbus, Ohio, 1985.
9. Rummel, R., Satellite altimetry in Geodesy and oceanography, Lecture Notes in Earth sciences 50, Springer-Verlag, New York, 1992.
10. Sailor, R.V. and M.L. Discoll, Noise model for satellite altimeter data, EOS (Am. Geophys. Union Trans.), Vol. 74, No. 16, 1993, pp. 99.
11. Sandwell, D.T., Antarctica marine gravity field from high-density satellite altimetry, Geophys. J. Int., vol. 109, 1992, pp. 437-448.
12. Wessel, P., and A.B. Watts, On the accuracy of marine gravity measurements, J. Geophys. Res., Vol. 93, No. B1, 1988, pp.393-413.